

Adsorption of polymers on a brush: Tuning the order of the wetting phase transition

Luis G. MacDowell^{a)}

Departamento de Química Física, Facultad de Ciencias Químicas, Universidad Complutense, 28040 Madrid, Spain

Marcus Müller

Institut für Theoretische Physik, Friedrich-Hund-Platz 1, Georg-August Universität, 37077 Göttingen, Germany

(Received 29 November 2005; accepted 10 January 2006)

We develop a computational methodology for the direct measurement of a wetting transition and its order via the effective interface potential. The method also allows to estimate contact angles in the nonwet state and to study adsorption isotherms. The proposed methodology is employed in order to study the wetting behavior of polymers on top of a brush consisting of identical polymers. In the absence of long-range forces, the system shows a sequence of nonwet, wet, and nonwet states as the brush density is increased. Including attractive long-range interactions we can make the polymer liquid wet the brush at all grafting densities, and both first- and second-order wetting transitions are observed. The latter case is limited to a small interval of grafting densities where the melt wets the brush in the absence of long-range interactions. Second-order wetting transitions are preceded by a first-order surface transition from a thin to a thick adsorbed layer. The interval of second-order wetting transitions is limited at low grafting densities by a surface critical end point and at high grafting densities by a tricritical wetting point. Our study highlights the rich wetting behavior that results when competing adsorbent-substrate interactions of different scales are tuned over a broad range. © 2006 American Institute of Physics. [DOI: [10.1063/1.2172597](https://doi.org/10.1063/1.2172597)]

I. INTRODUCTION

As a result of the increased ability to control and modify surface structure,¹ theoretical and computational works on wetting and adsorption have received abiding interest.²⁻⁸ Among the different materials considered, polymers are one of the most studied, because of their great versatility and practical interest (e.g., protective coatings). Moreover, the vapor pressure is vanishingly small for long chain molecules and evaporation effects can be neglected. Many properties such as structure, composition, or chain length may be varied during the synthesis providing control over the required wetting properties. Furthermore, polymers can also be adsorbed or irreversibly grafted onto substrates,⁹⁻¹¹ and the properties of the resulting brush may be further modified via the quality of the surrounding solvent.¹²

Although grafting polymers on a substrate is expected to increase the compatibility of polymer films because it adds attractive interactions to the substrate, it has been found that the brush's density plays an important role.¹³ For too high grafting densities of the brush (or large crosslink density of polymer networks), polymers of the same material as the brush have been found to be *autophobic*, i.e., the chemically identical molecules in the brush and the melt repel each other and the melt dewets from the brush.^{9-11,14} For smaller brush densities, however, suitably prepared brushes are known to enhance the wetting properties and reduce the contact angle of polymers that do not wet the bare substrate. In such

cases, a sequence of nonwet, wet, and nonwet states may be observed as the brush density is increased.^{11,15} The role of entropic factors in this wetting sequence has been emphasized,¹³ and several self consistent field theoretical studies have been devoted to the study of the autophobic regime.¹⁵⁻¹⁹

Obviously, the wetting properties of a film will also depend on the nature of the substrate where the brush is grafted. From an applied or experimental point of view, this provides further control over the system (e.g., by using a surface coating or a thin adsorbed layer one can modify the wetting behavior). From the theoretical point of view, one expects an intriguing interplay between forces that act on different length scales. (i) Short-range interactions that stem from the distortion of the narrow liquid-vapor or substrate-liquid interface. The width of these interfaces is dictated by the correlation length of density fluctuations ξ , which is on the order of the statistical segment length for dense polymer melts. (ii) There are weaker interactions in polymer melts that extend up to the size of the polymer coil, R_e .²⁰⁻²² For long polymer chains these two short-ranged contributions have well separated length scales, but for the rather short chains considered in our simulations we do not attempt to distinguish between the two contributions. (iii) There are truly long-range interactions that arise from the tails of the dispersion interactions between the polymer segments and the constituents of the substrate. The strength of these long-range power-law interactions is parametrized by the Hamaker constant A . In the case of a polymer layer on top of

^{a)}Electronic mail: luis@ender.quim.ucm.es

a polymer brush the distinction between long-range and short-range forces becomes particularly clear because the liquid-vapor interface does not come close to the substrate and difficulties in distinguishing between long- and short-range forces do not arise.

Interestingly, not only the intensity but also the attractive or repulsive character of long-range forces can be modified in some situations. In dewetting studies of polymers, these interactions could be greatly modified by coating the surface with an oxide layer of varying thickness. This control of the surface properties can lead to a new wetting behavior. Studies of polystyrene films adsorbed on silicon wafers show a two-stage dewetting process. At a high temperature, micrometer scale droplets are found on top of a uniform ultrathin film, a few nanometers thick. Upon cooling, rupture of the thin film is observed.^{23–25} This reveals a transition between two different equilibrium film thickness, none of which correspond to a fully wet state. A similar two-stage wetting process due to the interplay of short- and long-range interactions has been observed in studies of alkanes adsorbed at the air/water interface. Under suitable conditions, it is found that these systems exhibit a first-order surface transition between a thin and a thick film.^{26,27} This unexpected transition is then followed by a second-order or critical wetting transition, where the thickness of the film gradually diverges.²⁸

In this work we employ computer simulations in order to explore the wetting behavior of polymers on a brush consisting of grafted polymer of the same chemical nature and length. Interactions between polymer segments are considered to be strictly short range. The strength of the short-range interactions between polymer and substrate is modified by changing the grafting density of the brush. Laterally integrated Lennard-Jones interactions between polymer and substrate and the tails of the dispersive interactions between polymer segments that have been truncated in the model of the direct interactions result in long-range interactions. Their strength is controlled by an effective Hamaker constant A . Previously, this system was studied using self consistent field theory and a very rich wetting behavior was observed, exhibiting *inter alia* a two-stage dewetting process similar to that observed experimentally for polystyrene on silicon wafers and alkanes at the air/water interface.¹⁵

Despite this *a priori* information, the calculation of a wetting phase diagram by means of computer simulations is not a simple matter.²⁹ Even for simple Ising spin models the growth of the film thickness and the concomitant slow, long-wavelength fluctuations at weakly first- or second-order wetting transitions pose a challenge for simulations.^{29,30} In view of the much longer molecular relaxation times of polymeric materials we have only been able to investigate the wetting behavior of rather short chains utilizing advanced simulation and analysis techniques and a substantial amount of computer time. Here we propose a new technique which allows us to directly measure the effective interface potential, containing a wealth of information about the surface thermodynamics. A brief account of this technique was reported recently.³¹

Our manuscript is arranged as follows. In the next sec-

tion we introduce our coarse-grained polymer model and simulation methodology. Then we present our simulation results for the different regimes of the grafting density and analyze them within a simple phenomenological expression for the interface potential. Section IV contains our conclusions.

II. MODEL AND SIMULATION METHODOLOGY

A. Model system

We consider a simple coarse-grained polymer model which we have utilized previously.^{32–34} Polymers consist of a linear string of N beads, which interact with every other bead in the system by means of a truncated and shifted Lennard-Jones potential,

$$V_{LJ}(r) = \begin{cases} 4\epsilon \left\{ \left(\frac{\sigma}{r} \right)^{12} - \left(\frac{\sigma}{r} \right)^6 \right\} + \frac{127\epsilon}{4096}, & r \leq r_c \\ 0, & r > r_c, \end{cases} \quad (1)$$

where the truncation distance r_c is set equal to $r_c = 2 \times 2^{1/6} \sigma$. In the following, we will employ the Lennard-Jones diameter σ as unit of length and the Lennard-Jones potential depth ϵ as unit of energy, unless otherwise stated.

Contiguous monomers along the same chain additionally interact via a bonding potential of finite extensible nonlinear elastic (FENE) type,

$$V_{\text{FENE}}(r) = -kR_0^2 \ln \left(1 - \frac{r^2}{R_0^2} \right). \quad (2)$$

In the above equation the maximum allowed displacement between bonded monomers is $R_0 = 1.5\sigma$, while k , which plays the role of an elastic constant, takes the value $k = 15\epsilon/\sigma^2$.

Free polymers of the system are placed within a cuboidal simulation box, whose sides L_x , L_y , and L_z are such that $L_x = L_y$ and $L_z \gg L_x$. We impose periodic boundary conditions along the lateral x and y directions, and place perfectly flat walls at $z=0$ and $z=L_z$. Additionally, a number of n_g chains are grafted onto each wall. Their first monomers are located at $z_0 = 1.2$ and the grafting points are arranged on a square lattice with $1/\Sigma = n_g/(L_x L_y)$ being the number of grafted chains per unit area. The grafting substrate additionally interacts with the chain segments via a long-range potential of the form,

$$V_{\text{wall}}(z) = A \left\{ \text{sign}(A) \left(\frac{\sigma}{z} \right)^9 - \left(\frac{\sigma}{z} \right)^3 \right\}, \quad (3)$$

where z denotes the perpendicular distance of the polymer site to the closest substrate. A is the effective Hamaker constant characterizing all long-range interactions between substrate and polymer and the residual tails of the polymer-polymer interactions that are omitted by the truncation of the Lennard-Jones potential.

In the following grafted and free polymers are identical, and they are comprised of $N=10$ segments. The simulations are all carried out at the reduced temperature $k_B T/\epsilon = 1.68$. In terms of the monomer number density ϕ , the coexistence liquid and vapor densities are $\phi_l = 0.61$ and $\phi_v = 0.0083$, re-

spectively. The interface tension is $\gamma/k_B T = 0.0953$ and the mean end-to-end distance of the polymers is $R_e = 3.66$.³²

The optimal size of the simulation box has to meet two requirements. A large substrate area is needed for simulating low grafting density due to the small number of grafted chains. Additionally, L_z must be large enough such that the interfaces at $z=0$ and $z=L_z$ do not interact. Obviously, a too large system makes the simulations computationally infeasible and density fluctuations in the vapor might significantly contribute to the total density fluctuations. Typically we considered system sizes with L_x between 14σ for the low grafting densities and 8σ for the highest grafting densities. In order to avoid interaction of the two interfaces, we typically employed $L_z = 90\sigma$, but occasionally $L_z = 180\sigma$ was required for simulating very thick films. The number of grafted chains on a wall varied between $n_g = 16$ for the lowest grafting densities and $n_g = 36$ for the highest grafting densities.

A symmetric simulation box with two identical substrates allows to gather statistics from both halves of the simulation. In practice, however, having two brush-covered substrates results in very large relaxation times, in particular, when thick liquid films form. Therefore, we often use a purely repulsive substrate at $z=L_z$ to sample the fluctuation of a single liquid-vapor interface, to reduce possible correlations, and to obtain better statistics.

B. Simulation methodology

Locating a wetting transition by computer simulation poses a challenge because of the divergence of the thickness of the liquid film at the transition. Both, protracted long equilibration times as well as significant finite size effects, have to be accounted for.

An accurate method to locate first-order wetting transitions consists in calculating the surface free energy difference of the liquid and vapor in contact with the substrate and the liquid-vapor interface tension in separate simulations. Then, the Young equation is utilized to calculate the macroscopic contact angle and to locate the wetting transition. This method is particularly advantageous at strong first-order transitions because the thickness of the fluid layer at the nonwet substrate virtually vanishes which strongly reduces finite size effects.³²

This method, however, gradually becomes more difficult as the strength of the wetting transition decreases. Although the liquid layer in the nonwet state remains microscopic it comprises several molecular diameters and the relaxation times of long-wavelength fluctuations of the film thickness are protracted long. Moreover it is difficult to estimate the strength of the first-order transition from the analysis of the surface and interface tensions that enter Young's equations.

An alternative is to directly measure the interface potential in the simulations. The interface potential $g(l)$ measures the free energy of a liquid film per unit area as a function of its thickness l or another suitably defined measure of the substrate adsorption. This interface potential or the concomitant disjoining pressure can also be measured experimentally, but the experiments are only able to probe a limited region corresponding to rather large film thickness.^{35,36} If we nor-

malize g such that $g(l \rightarrow \infty) \rightarrow 0$, the knowledge of the film thickness where the interface potential exhibits its global minimum l_{\min} allows us to measure the contact angles, because then

$$\gamma_{LV}(1 - \cos \theta) = g(\Gamma = \infty) - g(\Gamma_{\min}) = -g(\Gamma_{\min}), \quad (4)$$

where Γ_{\min} is the adsorption at the minimum of g . Furthermore, g contains information on the order of the transition and the stability of thin films.

In order to measure free energy differences we perform Monte Carlo simulations in the grand canonical ensemble. In this way, we are able to monitor the probability of finding a given number of polymers within the system. Since the grand potential of a state with n particles is directly proportional to $-k_B T \ln P(n)$, the probability distribution allows us to directly calculate the free energy differences. To be more specific, we would like to estimate the interface potential by monitoring the probability $P_{1/2}(n)$ of finding n polymers inside the half of the simulation box that contains the brush-covered substrate. We can then define a surface adsorption Γ as the total number of monomers in that half box $n_{1/2}$ less the amount found in an equal bulk volume, i.e.,

$$\Gamma = \left(N n_{1/2} - \frac{1}{2} \phi_v V \right) / L_x L_y. \quad (5)$$

In this way, we can determine the interface potential as

$$g(\Gamma) = - \frac{k_B T}{L_x L_y} \ln P_{1/2}(\Gamma). \quad (6)$$

To a crude approximation the interface excess is related to the thickness l of a uniform liquid film via $\Gamma = \Delta \phi l$ with $\Delta \phi = \phi_l - \phi_v$. This approximation assumes a sharp, rectangular density profile at the substrate and the liquid-gas interface and it neglects that density fluctuations in the bulklike regions of the profile. Thus, plotting the interface profile versus $\Gamma / \Delta \phi R_e$ yields an approximation for the interface potentials as a function of the film thickness in units of the end-to-end distance, R_e .

This procedure poses both conceptual and technical challenges. If we fix the lateral system dimensions, L_x and L_y , of our cuboidal simulation cell, and increase the perpendicular distance L_z , the interface of a thick film at coexistence will not be bound to the substrate and will wander around as to explore the whole volume. In the limit $L_z \rightarrow \infty$ there is no stationary probability distribution even if $g(l)$ has a finite minimum binding the interface to the substrate. In order to obtain a meaningful normalizable probability distribution one first has to consider the limit $L_x, L_y \rightarrow \infty$ and then can consider the limit of large film thickness, $L_z \rightarrow \infty$. The fact that the interface explores the whole volume of the system is also a technical problem because it imparts extremely long correlation times of interface fluctuations and the simulation spends a lot of time exploring regions where the interface and the substrate do not interact and the interface potential is flat.

A simple remedy is to simulate at slight undersaturation,³⁰ $\Delta \mu = \mu - \mu_{\text{coex}}$. In this case the effective interface potential $g_{\Delta \mu}$ is exactly obtained as described above but

large film thicknesses are suppressed and the interface always returns to the substrate. The interface potential at coexistence as defined in Eq. (6) is simply recovered by means of a Legendre transformation,

$$g_0(\Gamma) = g_{\Delta\mu}(\Gamma) - \Gamma_f \Delta\mu, \quad (7)$$

where Γ_f is the adsorption of free chains (as opposed to Γ , the adsorption of both grafted and free chains).

This procedure works well if g_0 exhibits only a shallow minimum (wet, small contact angle or weakly first-order transition). In the opposite case, g_0 showing a deep well (large contact angle or strongly first-order transition), the simulation explores only the narrow region where the interface is bound to the substrate and it is difficult to extract the limit $l \rightarrow \infty$ from the simulation data. In order to avoid this problem we utilize successive sampling,³⁷ a variant of the well known umbrella sampling technique.³⁸

In our simple implementation of successive sampling, we perform standard grand canonical simulations but rather than sampling over the actual grand canonical probability distribution $P(n)$ for a given temperature T and chemical potential μ , we subdivide the interesting interval of the number of chains into overlapping subintervals, $[n_{i-1}, n_i]$. Monte Carlo moves that try to leave the interval are rejected as to fulfill detailed balance at the boundaries. Performing different simulations in the subintervals we obtain an estimate of the distribution $P_i(n)$ in the i th subinterval. Then, the results of the subintervals are matched at their boundaries to provide an estimate for the grand canonical distribution function over the entire range of the number of chains. Let n be in the interval $[n_i^-, n_i^+]$ and n' be in the neighboring interval $[n_{i-1}^-, n_{i-1}^+]$ which overlap at \bar{n} , then

$$\frac{P(n)}{P(n')} \approx \frac{P_i(n) P_{i-1}(\bar{n})}{P_i(\bar{n}) P_{i-1}(n')}. \quad (8)$$

Successively we construct an estimate for the unnormalized distribution, $P(n)$, for all the considered n relative to some arbitrarily chosen probability, $P(n_0)$.

Actually, $P(n)$ contains information on two interfaces, that at $z=0$ and that at $z=L_z$. The interface potential of one such substrate is determined from $P_{1/2}(n)$, the probability of obtaining n particles in the corresponding half box. This information may be recovered by monitoring $P_{1/2}(n|k)$, the probability of finding n particles in a half box, given that the total number of polymers within the box is k . This conditional probability is independent of the chemical potential and may be measured during the simulations. At the end of the simulation, we calculate the information as

$$P_{1/2}(n) = \sum_{k=n}^{\infty} P(k) P_{1/2}(n|k). \quad (9)$$

In principle, all states of the system with more than n molecules will contribute to the summation. In practice, obtaining meaningful probabilities for very large n is not feasible. Fortunately, it was found that the sum converges fairly fast (cf. Fig. 1) and could be truncated, provided the convergence is carefully monitored. Typically, we studied a range of 250 molecules divided in about five subintervals with 50 particles

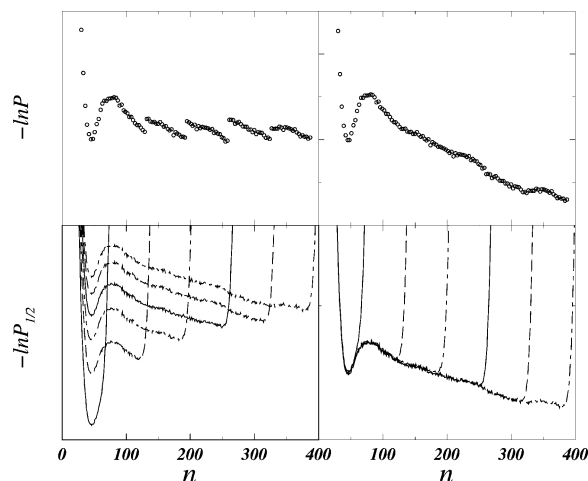


FIG. 1. Calculation of interface potentials. Top figures show the probability of finding n molecules inside the whole simulation box at $k_B T / \epsilon = 1.68$ and the coexistence value of the chemical potential. Top left panel presents the piecewise distributions obtained within each window. Top right panel is the resulting distribution obtained after matching the piecewise functions. Bottom figures show the probability distribution of finding n molecules a distance less than $L_z/2$ away from the substrate. Left panel illustrates the cumulative distributions that are obtained as an increasing number of windows is considered. Right panel shows how the cumulative distributions in the left collapse into a single master curve, the interface potential.

each, but the number of subintervals required can be increased as needed.

Figure 1 illustrates the methodology proposed for the calculation of interface potentials. The top left panel shows the partial distributions P_i obtained within each window. Shifting the logarithms of the piecewise probability distributions according to Eq. (8) as to match them in the overlapping windows we obtain a continuous function $P(n)$, independent of the specific choice of subintervals employed (top right). For each of the windows, we also monitor the conditional probabilities which, using Eq. (9), allow us to estimate $P_{1/2}(n)$. A distribution obtained in this way from i successive windows shows a spurious increase close to the maximum number of particles allowed in the system, i.e., n_i , due to truncation effects in Eq. (9). However, increasing the number of windows employed allows to shift the spurious feature to larger particle numbers as desired (bottom left), and the resulting distributions differ by a simple additive normalization constant within the unperturbed interval (bottom right).

From the knowledge of the interface potentials, we can determine several interface properties, including the value of the effective Hamaker constant A_{wet} at which the liquid wets the brush. We estimate the location of first-order wetting transitions using two different methods. First, we plot $P_{1/2}(n)$ for a system slightly above a first-order wetting transition. The probability distribution is bimodal and by decreasing the bulk chemical potential, $\Delta\mu_{\text{pw}} = \mu_{\text{pw}} - \mu_{\text{coex}} < 0$, into undersaturation the area below the two peaks can be made equal. The equal weight rule of phase coexistence³⁹ asserts that at this undersaturation and substrate interaction, A , a thin and a thick film thickness coexist with each other. In contrast to the wetting transition itself, only finite layer thickness is involved and finite size effects can be controlled. This prewetting coexistence is the hallmark of a first-order wetting tran-

sition. Once the line of prewetting points (A, μ_{pw}) has been determined we estimate the location of the wetting transition by extrapolating the prewetting line back towards the coexistence chemical potential according to^{32,40}

$$\Delta\mu \propto (A - A_{wet})^{3/2}. \quad (10)$$

Thus, a fit to the available data for the prewetting line allows us to accurately estimate A_{wet} .

The calculation of the prewetting line as described above becomes difficult for systems with small lateral size because the tail of the peak that corresponds to a thick film decays as $\exp(-L_x L_y \Delta\mu\Gamma/k_B T)$. For small system sizes this tail decays very slowly and acquires a large weight. In large systems, the states between fully developed thin and large systems consist of coexisting thin and thick films, with an extra energy penalty arising from the line tension λ . The line between the films will run across the smallest lateral dimension, either L_x or L_z , and will have a total cost $\lambda \min(L_x, L_y)$. For small systems, however, this contribution is relatively small, and the minimum of the probability distribution between the two stable peaks is not very well developed. In such cases, we determine the wetting transition by direct inspection of the interface potential, i.e., by estimating the substrate interaction at which $g(\Gamma_{min})=0$, where Γ_{min} is the adsorption at the minimum of the interface potential. This procedure is reminiscent of locating the prewetting via the equal height rule (instead of the equal weight rule), and we expect stronger finite size effects.

Since the calculation of full interface potentials is rather time consuming, it is desirable to exploit the data obtained during a simulation as much as possible. In the course of this study, extrapolation of one calculated interface potential in order to predict interface potentials for other values of A and T is very useful. The expressions required for this histogram extrapolation⁴¹ are obtained by writing the grand canonical probability of observing a given number of particles as follows:

$$P_{\mu VT}^A(n) \propto \exp(\mu n/k_B T) Q_{nVT}^A, \quad (11)$$

where Q_{nVT}^A is the canonical partition function of a system with Hamaker constant A . The probability distribution for another value of the Hamaker constant A' can be expressed by the previous distribution,

$$P_{\mu VT}^{A'}(n) \propto P_{\mu VT}^A(n) \frac{Q_{nVT}^{A'}}{Q_{nVT}^A}. \quad (12)$$

Noting that the wall energy of a given microcanonical configuration differs in both systems by a multiplicative factor A/A' only, the ratio of canonical partition functions may be written as

$$\frac{Q_{nVT}^{A'}}{Q_{nVT}^A} = \frac{\int e^{-\beta(A'/A-1)\Phi} e^{-\beta(U+\Phi)} d\mathbf{r}^n}{\int e^{-\beta(U+\Phi)} d\mathbf{r}^n}, \quad (13)$$

where U is the sum of all pair interactions, while Φ is the sum of all wall-monomer interactions. The equation above has been arranged in a manner such that its resemblance with perturbative free energy calculations is made explicit. Noting

that $\exp(-\beta(U+\Phi))$ may be considered as a probability density, we obtain³²

$$P_{\mu VT}^{A'}(n) \propto P_{\mu VT}^A(n) \langle \exp(-(A'/A-1)\Phi/k_B T) \rangle_A, \quad (14)$$

where the average is performed over a canonical distribution with Hamaker constant A . This expression means that averages corresponding to the thermodynamic states μ, V, T , and A' can be constructed from a sample of microstates generated (according to the Boltzmann weight) at the states μ, V, T , and A by assigning each microstate the weight $\exp(-(A'/A-1)\Phi/k_B T)$.

An important point regards our order parameter, the adsorption Γ . This corresponds to the integral criterion for locating the position of the liquid-vapor interface, but other schemes based on the detailed knowledge of the profiles (crossing criteria) can also be utilized to determine the film thickness l .^{42,43} Moreover, monitoring the adsorption we cannot distinguish between the formation of a uniform layer and a droplet. At a fixed adsorption the system will adopt the configuration that minimizes the free energy—be it a uniform film, two coexisting films of different thickness, or a droplet. This can be verified explicitly via configurational snapshots. The configurations that a system adopts at fixed excess number of particles and their dependence on the system size have been discussed both for thin films on substrates⁴⁴ as well as for the periodic simulation cells (i.e., bulk simulations).^{45,46} In the latter cases (coexistence between two different film thicknesses or a droplet), the measured probabilities will not be simply related to the interface potential but contain additional information about the line tension.^{44,47} Importantly, states that correspond to the minima of the interface potential (i.e., the configurations that are pertinent to the equilibrium wetting behavior) will correspond to laterally uniform configurations and free energy differences between these states have the usual meaning.

III. RESULTS

Figure 2 shows the interface potentials for brushes of increasing grafting density in the absence of long-range forces, i.e., $A=0$. As expected, for low grafting densities the interface potential shows a rather deep minimum at low adsorption. Due to steric reasons, the almost bare surface greatly reduces the configurational entropy of chains close to the substrate, and a thick film is not stable. Actually, for a bare hard surface, previous results for the same model suggest a drying transition at $A=0$.³² Gradually increasing the brush density we decrease the depth of the minimum. As a result of attractive interactions, grafting chains on the substrate somewhat compensate for the loss of entropy. Eventually, at intermediate grafting densities the interface potential becomes a monotonically decreasing function of the adsorption, and no trace of a minimum remains. This shows that the attraction provided by the grafted chains can lead to wetting even in the absence of long-range forces. However, upon further increasing the grafting density, the brush becomes so dense that penetration of the chains is at a great cost and the system dewets. The dewetting of a fluid on top of a substrate made of the same kind of molecules is known as *autopho-*

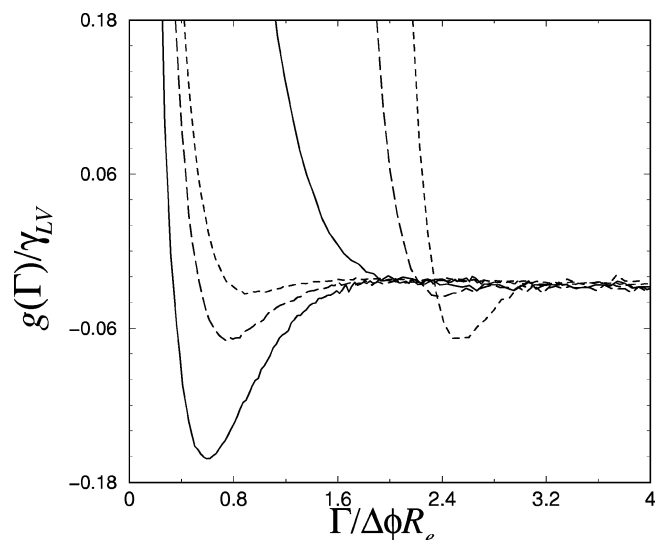


FIG. 2. Interface potentials $g(\Gamma)$ as a function of the total adsorption Γ for several brush densities and $A=0$. From left to right, $g(\Gamma)$ of increasing grafting densities, and $R_e^2/\Sigma=1.09$ (full line), 1.23 (long dashed), 1.31 (short dashed), 2.68 (full), 5.63 (long dashed), and 6.70 (short dashed).

bicity, a phenomenon which has been studied both experimentally^{10,11,14} and theoretically.^{16–19}

It would be interesting to relate the equilibrium adsorption (i.e., minimum of the interface potentials) to the well known properties of the system, such as end-to-end distance, grafting density, and wall strength. For extremely simplified models—assuming incompressible brushes, no enthalpic interactions, and Gaussian distribution of polymers—analytic expressions may be obtained.¹³ However, for the short polymers considered here, typical polymer scaling laws are only qualitatively obeyed. Both short-range and long-range interactions must be considered, and packing effects on the monomer length scale are relevant. A simple relation between equilibrium film thickness and fluid polymers is therefore not available, but self consistent field theories may be employed to obtain numerical estimates of the interface potential.^{15–19}

The interface potential in the absence of long-range forces allows us to classify the behavior into three regimes: sparsely grafted brushes, ranging from $R_e^2/\Sigma=0$ to 1.34, show a behavior similar to that of a bare substrate. The attraction provided by the grafted chains is not enough to stabilize a thick polymer film and the system remains nonwet. Brushes with intermediate grafting density, ranging from $R_e^2/\Sigma=1.34$ to about $R_e^2/\Sigma=5.36$, show a monotonically decreasing interface potential, i.e., the polymer melt wets the brush. Finally, for high grafting densities, beyond $R_e^2/\Sigma=5.36$, the brush is so dense that liquid films become again unstable and autophobic dewetting occurs.

The existence of different regimes and their behavior may be intuitively explained and rationalized by inspecting the polymer density profiles of the system. Figures 3–5 show the density profiles for brushes in each of the three regimes. Each of the plots includes the results for three different film thicknesses: (1) a bare brush ($\Gamma=\Gamma_g$), (2) a thin film that corresponds to the equilibrium adsorbed amount (i.e., the minimum of the interface potential, $\Gamma=\Gamma_{\min}$), and (3) a thick

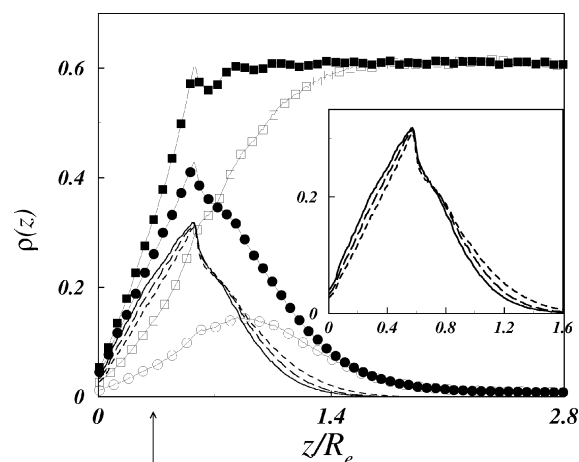


FIG. 3. Density profiles for a brush of low grafting density, $1/\Sigma=0.0816$, with three different adsorptions, corresponding to a bare brush, a brush at the minimum of the interface potential, and a brush at a (large) plateau value of the interface potential. The lines are the density profiles of grafted chains (full, bare brush; long dashed, brush at minimum; dotted, brush at plateau). The empty symbols correspond to the free chains (circles, brush at minimum; squares, brush at plateau). The filled symbols correspond to the total (graft+free) density profiles (circles, brush at minimum; squares, brush at plateau). The arrow on the z axis marks the position of the first monomers of the grafted chains which have been excluded from the density profiles. The inset shows the detail of density profiles for the grafted chains.

liquidlike adsorbed film, corresponding to the asymptotic part of the interface potential ($\Gamma=\Gamma_\infty$). For each situation, we consider the density profile of grafted polymers $\rho_g(z)$ (full lines), that of free chains $\rho_f(z)$ (dashed lines), and the resulting total density profile $\rho_t(z)$ (symbols). The contribution of the first monomer of grafted chains is a sharp peak at $z_0=1.2$ which is not included but marked by an arrow on the horizontal axis.

Figure 3 shows the density profiles for a brush with $R_e^2/\Sigma=1.09$ in the low density regime. The density profile for the bare brush vanishes at the substrate and exhibits a maximum around $z \approx 0.6R_e$. For the short chain length considered, however, the different length scales—segment size σ , that

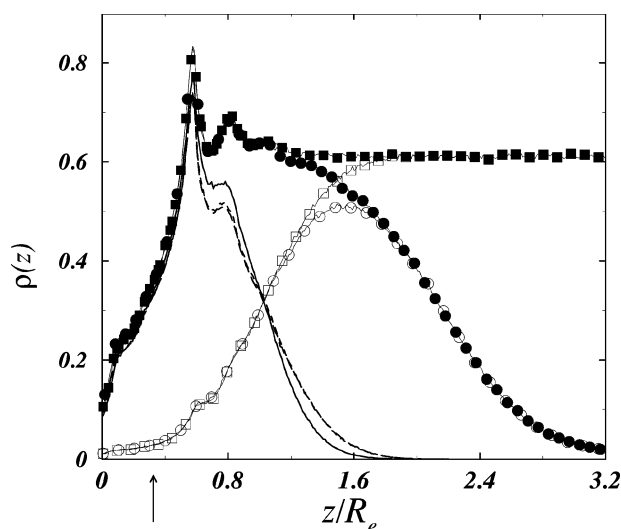


FIG. 4. Density profiles for an intermediate grafting density brush, $1/\Sigma=2.68$. Symbols as in Fig. 3. The density of the grafted chains for Γ_{\min} and Γ_∞ looks equal on the scale of the graph.

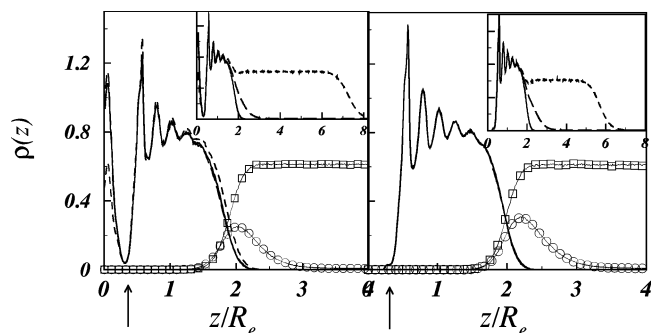


FIG. 5. Density profiles for a dense brush, $R_e^2/\Sigma=6.70$ at $A=0$ (left) and $A=1.2$ (right). Symbols as in Fig. 3, except for total density profiles, which are shown in the inset: long dashed line, brush at the minimum; short dashed line, brush at the plateau. The grafted chain density profile (full line) is also included in the inset for comparison. The arrow on the z axis marks the position of the first monomers of the grafted chains which have been excluded from the density profiles.

determines the packing, excluded volume screening length ξ , that characterizes density correlations, and the molecular size R_e —are not well separated. The maximal density is much lower than the liquid density ϕ_l . The profile results from a balance between attractive interactions, promoting the collapse of chains, and conformational entropy, penalizing the compression of chains into an ultrathin film.

Adding a small amount of free chains to this brush decreases the free energy, for the free chains help building a uniform layer and thus reduce the stretching of the grafted chains. As can be observed from the profile, the laterally averaged surface to the vapor sharpens and gradually adopts the shape of a narrow liquid-vapor interface.

In Fig. 4 we show the density profiles observed for a brush $R_e^2/\Sigma=2.68$ characteristic of the intermediate density regime. The brush is now considerably more dense and some density oscillations (packing) in $\rho_g(z)$ already occur in the bare brush. However, the density is not so large as to prevent free polymers to penetrate the brush. Therefore, increasing the adsorption decreases the overall free energy, and the maximum possible penetration occurs for $\Gamma \rightarrow \infty$. There is an extremely shallow minimum in the interface potential which is beyond the statistical accuracy of our simulations and its is therefore disregarded in the following discussion.⁴⁸

The autophobic dewetting at high grafting densities may be understood from the resulting density profiles shown in Fig. 5 (left) for a brush with $R_e^2/\Sigma=6.70$. In this case, the very dense brush results in a highly packed and structured brush, as revealed by $\rho_g(z)$ for the bare brush. The brush is stretched and the density of brush segments is typically higher than that of the liquid at coexistence. Thus, only a very limited amount of the free polymers can penetrate the brush and the adsorption Γ_{\min} is very small. It is just sufficient to make the surface of the bare brush adopt the shape of a narrow liquid-vapor interface. When more chains are added, they are confined to the top of the brush. Since the penetration is so small, they do not sufficiently benefit from attractive interactions with the brush, but suffer a rather large entropy loss due to the steep density gradient at the brush-melt interface.

The previous discussion is based on the analysis of the

density profiles as a function of perpendicular distance to the substrate. Therefore, the in-plane structure is averaged out. In bad solvents both simulations^{49,50} and experiments⁵¹ observe that sparsely grafted brushes do not form a laterally homogeneous dense layer but rather form dimples whose characteristic lateral size is dictated by R_e . This effect has not been observed in our self consistent field theory (SCFT) calculations,¹⁵ which assumed a laterally homogeneous profile from the outset.

In our simulations we find that for very low grafting density at each instant in time large patches of the substrate are not covered by the brush, i.e., there are strong density fluctuations. The assumption of a spatially homogeneous density in the lateral direction is only a very crude description of the system. As we increase the grafting density, however, the spatial inhomogeneity decreases. Note that our chain length is rather short and that the temperature is not very far below the Θ point, $T/\Theta \approx 0.51$. For brushes with $R_e^2/\Sigma \geq 1.09$, the lateral structure of density profiles is mainly due to the first two monomers of the grafted chains, the remainder of the chain producing a rather uniform background.

In order to relate the structure of the brushes and the adsorbed films with the wetting behavior, it is also important to consider the effect of changing the Hamaker constant. Clearly, the long-range wall potential may influence the wetting behavior as a result of interactions with the adsorbed film, but also indirectly via the influence on the brush structure. For dense brushes, however, the effect is fairly small, because the brush is so compact anyway. Figure 5 (right) shows the density profiles for a brush with $R_e^2/\Sigma=6.70$ and $A=1.2$. Comparison with results for $A=0$ shows that the structure remains rather similar. Actually, the only significant difference results from the z^{-9} repulsive part of the long-range potential [cf. Eq. (3)], which expels the first few brush monomers away from the neighborhood of $z=0$. The much longer range contribution, z^{-3} has almost no effect and does not produce qualitative changes of the in plane structure.

The limit of a dry, dilute brush is more rich and has been investigated for a similar model both below^{50,52} and above the theta temperature.⁵² In such cases, the resulting structure is laterally inhomogeneous and density profiles as a function of the perpendicular distance to the wall do not provide a complete description of the brush.

After this qualitative discussion of the density profiles, we now study the nature of the wetting transitions that occur in each of the three regimes, and the effect of long-range forces.

A. Low grafting densities

Previously, we have studied the wetting behavior of our model polymer on a flat surface without brush.³² We found that the polymer fluid will wet the substrate if the Hamaker constant is larger than the wetting value $A_{\text{wet}}=3.22$. We expect that grafting chains on the substrate will increase the extent of attractive interactions, i.e., a wetting transition below $A_{\text{wet}}=3.22$ can be anticipated.

In Fig. 6 we show the interface potentials obtained for a

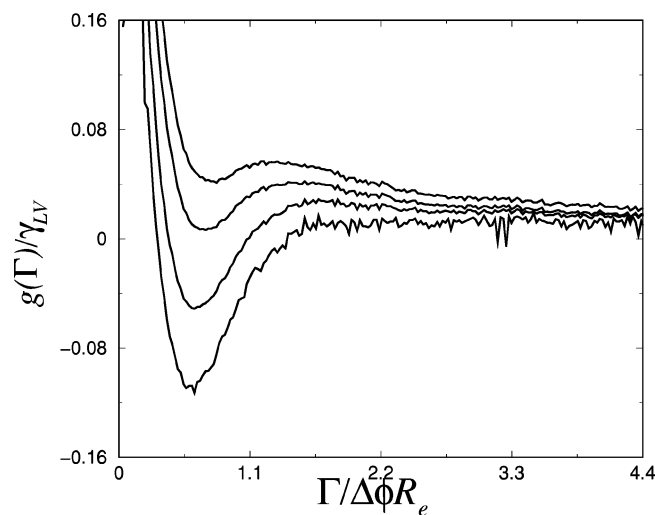


FIG. 6. Interface potentials as a function of total adsorption for a brush of density $R_e^2/\Sigma=1.09$ and several values of the Hamaker constant. From bottom up, $A=0.3, 0.5, 0.7,$ and 0.85 .

grafting density $R_e^2/\Sigma=1.09$ and increasing values of the Hamaker constant. For small Hamaker constants, $g(\Gamma)$ exhibits a rather deep minimum at low adsorption. The depth of the minimum gradually decreases as we increase the Hamaker constant. Eventually, the minimum becomes metastable, i.e., a film of infinitely large adsorption is stabilized and the melt of free chains wets the brush. From the interface potential we infer the location of the wetting transition at about $A_{\text{wet}}=0.7$, well below $A_{\text{wet}}=3.22$. Furthermore, the structure of the interface potentials, with a well developed maximum separating thin and thick films, shows that the wetting transition is of first order.

As we increase the grafting density, the value of $A_{\text{wet}}(R_e^2/\Sigma)$ gradually decreases. Indeed, from Fig. 2 we expect that for large enough R_e^2/Σ the brush becomes wet for $A=0$. Therefore, the line of first-order wetting transitions eventually intersects the $A=0$ axis. Figure 7 shows a sequence of interface potentials calculated in the absence of long-range forces as the wetting transition is brought about by increasing R_e^2/Σ . In order to assess how close these three systems are from the wetting transition, we calculate the corresponding contact angles according to Eq. (4).

The values obtained for the three brushes of Fig. 7 are $16^\circ, 12^\circ,$ and 6° , for grafting densities $R_e^2/\Sigma=1.23, 1.28,$ and 1.31 , respectively, i.e., these brushes are very close to the wetting transition. Unfortunately, the statistical accuracy of our simulation data is not sufficient to decide whether or not a maximum that separates the nonwet state at Γ_{min} and a macroscopic thick film persists as we increase the grafting density. Such a maximum would indicate that the wetting transitions remain first order.

Despite this difficulty, we point out two strong features in favor of a first-order phase transition. First, if a second-order wetting transition occurred, we would expect the minima to gradually shift towards macroscopic adsorption. For this reason we mark the location of the minima Γ_{min} with an X in Fig. 7. For short-range forces Γ_{min} logarithmically

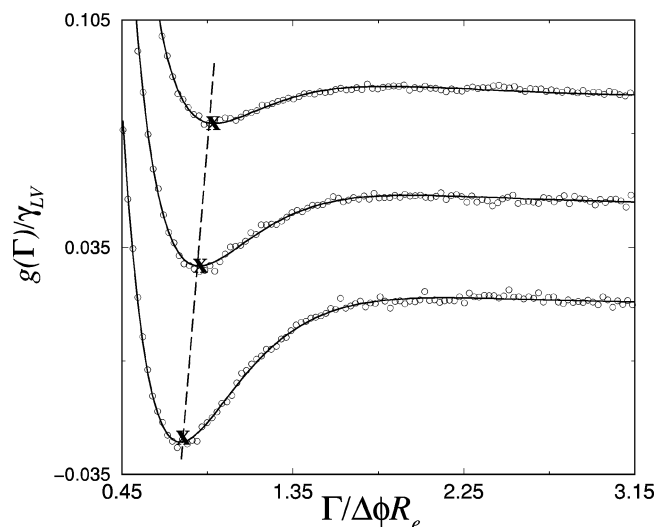


FIG. 7. Interface potentials as a function of the total adsorption for $A=0$ and several grafting densities approaching the wetting transition. From bottom up, $R_e^2/\Sigma=1.23, 1.28,$ and 1.31 . The symbols show the simulation results. The full lines are fits to the data (see text). The symbols “X” mark the location of the minima. The dashed line connects all such points and shows no evidence of divergence.

diverges upon approaching a second-order wetting transition⁴⁰ but this is not at all what we observe in our simulations.

Second, we study the shape of the interface potential as the wetting transition at $A=0$ is approached. From theoretical considerations, we expect that an interface potential for a system with short-range forces be described approximately by a sum of exponentials,⁴⁰

$$\beta g(\Gamma) = \sum_{k=1}^{\infty} C_k e^{-k\Gamma/\kappa}, \quad (15)$$

where C_k are coefficients depending on the properties of the substrate (i.e., the grafting density), while κ is a constant that only depends on the nature of the fluid. For such a model, the first few coefficients of the above expansion vary continuously with the system parameters. A minimal model of a second-order wetting transition requires two coefficients: C_1 positive and C_2 negative, with the latter exactly changing sign at the wetting transition. The simplest possible description of a first-order phase transition with the above model consists of a positive C_1 , a negative C_2 , and a third, positive coefficient C_3 .

We performed nonlinear regression analysis for the interface potentials using this simple model. A sum of three exponentials provides an excellent fit to the simulation results (see Fig. 7), while a sum of two exponentials yields a clearly unsatisfactory fit with root-mean-squared deviations that are about twice as large (fit not shown). Furthermore, taking into account that the parameter κ is related to the bulk correlation length via $\kappa=\xi(\phi_l-\phi_v)$, the fit suggests $\xi=2.24\sigma=0.61R_e$ which corresponds to the length scale of density fluctuations in the liquid or the intrinsic width of the liquid-vapor interface (without capillary waves).

TABLE I. Results for the fit of interface potentials to Eq. (15). Top: values of the coefficients a_k and b_k obtained from the fit to the linear model $C_k = a_k + b_k R_e^2/\Sigma$ (a value of $\kappa = 1.350\,263$ is obtained for the decay rate of the exponentials). Bottom: values of the preexponential terms C_k obtained for the three interface potentials employed in the fit.

	1	2	3
a_k	-0.021 54	-0.9662	0.7576
b_k	0.027 82	0.5977	-0.2255
R_e^2/Σ	C_1	C_2	C_3
1.230	0.012 68	-0.2312	0.4803
1.278	0.014 02	-0.2024	0.4694
1.307	0.014 84	-0.1848	0.4628

Furthermore, we can exploit the fit in order to estimate the actual location of the transition which is dictated by the condition,

$$C_2^2 = 4C_1C_3. \quad (16)$$

Assuming a linear dependence of C_k on the grafting density (see Table I), we estimate that the liquid will wet the brush for grafting densities larger than $R_e^2/\Sigma = 1.334$ in the absence of long-range forces ($A=0$).

B. Intermediate grafting densities

Next we consider the behavior for grafting densities larger than $R_e^2/\Sigma = 1.334$, where the brush is wet already in the absence of long-range forces. Including long-range forces with a positive Hamaker constant will make the adsorption of a thick film even more favorable and the melt will wet the brush. However, including repulsive long-range forces, $A < 0$, we destabilize thick films. In that case, the interface potential will exhibit an extra monotonously increasing contribution whose leading term takes the form $g \propto -\Gamma^{-2}$. Thus, no macroscopically thick film is stable for $A < 0$. The competition between a monotonously decreasing short-ranged contribution of the interface potential and the monotonously increasing negative contribution from the long-range contributions produces a second-order wetting transition as A changes sign.⁴⁰

Figure 8 presents the interface potentials for a brush with grafting density $R_e^2/\Sigma = 2.68$ and various Hamaker constants. For $A=0$, the interface potential is a monotonically decreasing function of the adsorption. As the Hamaker constant decreases, however, a shallow minimum appears and the corresponding adsorption Γ_{\min} decreases with A . In order to illustrate that the appearance of the minimum stems from the effect of long-range forces, we consider the contribution of the segment-substrate interaction, Eq. (3), to the interface potential within the sharp-kink approximation,

$$g_{\text{ir}}(l) = |A|(\phi_l - \phi_v) \left\{ \frac{1}{8} \left(\frac{\sigma}{l} \right)^8 + \frac{1}{2} \text{sign}(A) \left(\frac{\sigma}{l} \right)^2 \right\}, \quad (17)$$

where we have assumed a film thickness, $l = \Gamma/(\phi_l - \phi_v)$. The leading term of order Γ^{-2} is plotted in Fig. 8 and compared with the tails of the computed interface potentials; the con-

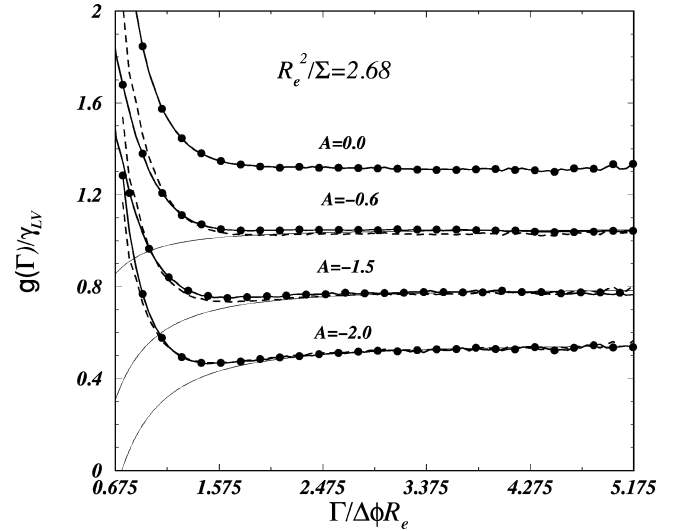


FIG. 8. Interface potentials as a function of the total adsorption for a brush of grafting density $R_e^2/\Sigma = 2.68$ and several (negative) values of A as indicated in the figure. Lines with circles: simulation results. Full black lines: long-range contribution of the interface potential as obtained from the sharp-kink approximation. Dashed lines: superposition approximation, obtained as a sum of $g(\Gamma)$ at $A=0$ and the calculated long-range contribution.

tribution in Γ^{-8} is extremely small and can be neglected for $\Gamma/R_e\Delta\phi < 0.5$. In all cases, the agreement between the model and the simulations is good. In the same figure we show interface potentials obtained by adding the computed $g(\Gamma)$ for $A=0$ and Eq. (17) (dashed lines). In all cases the agreement is again very good, supporting the superposition approximation employed in previous work.²⁴

At low grafting densities, a sufficiently large A produces a first-order wetting transition. For intermediate grafting densities, we have shown evidence for a critical, second-order wetting transition as A changes sign. Both regimes are separated by a critical end point located at $R_e^2/\Sigma = 1.334$. The question then arises in which form the first-order transitions continue beyond $R_e^2/\Sigma = 1.334$. Unfortunately, the wetting transitions observed as the grafting density approaches $R_e^2/\Sigma = 1.334$ are so weakly first order, that a direct monitoring of the interface potential with sufficient accuracy becomes very difficult: the possible maximum will be hardly detectable within the statistical uncertainty of our simulations. Therefore, we exploit the smooth dependence of the coefficients in the simple model of the interface potential, Eq. (15), in order to explore the wetting behavior in the vicinity of the critical end point. A simple analysis shows that the interface potential will exhibit a minimum followed by a maximum as long as $C_2^2 - 3C_1C_3 \geq 0$. Thus, for an appropriate value of $A < 0$ there is a coexistence between a thin and a thick liquid layer on top of the brush. Note that this continuation of the line of first-order wetting transition differs from prewetting because it occurs at bulk coexistence and not at undersaturation. The unfavorable long-range interactions play a similar role as the shift of the chemical potential from the bulk coexistence value in prewetting, i.e., they limit the growth of a macroscopically thick wetting layer. Our extrapolation shows that the above condition is fulfilled for $R_e^2/\Sigma \leq 1.3670$, just slightly above the predicted wetting

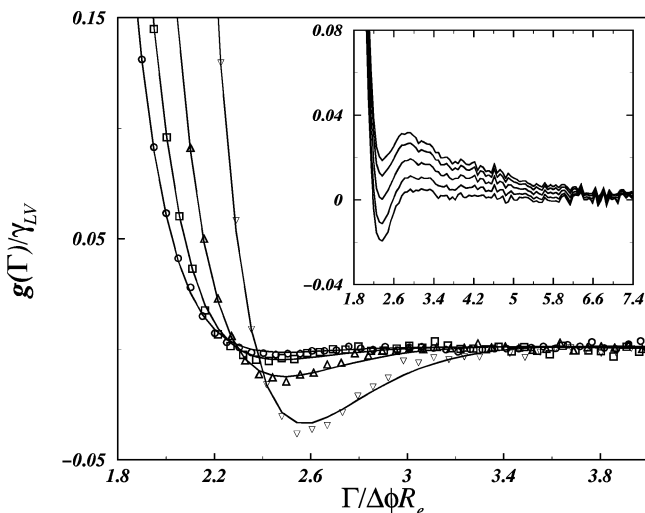


FIG. 9. Interface potentials slightly beyond the autophobic dewetting transition. The symbols are the results from simulation (circles, squares, up triangles, and down triangles correspond to $R_e^2/\Sigma=5.36, 5.63, 6.03,$ and 6.70 , respectively). The lines are a fit to the three exponential model, Eq. (18). The inset shows a series of interface potentials for a brush $R_e^2/\Sigma=6.03$ as A is increased, from bottom to top, $A=0.6, 0.8, 1.1, 1.4,$ and 1.6 .

transition at $R_e^2/\Sigma=1.334$. Beyond this grafting density the two minima structure disappears, i.e., the line of thin-thick transitions at the coexistence ends in a critical point. Fluctuations which are neglected in the mean field type of extrapolation are expected to considerably shorten the line of thin-thick transitions and the critical point at the end of the coexistence line will exhibit two-dimensional (2D) Ising critical behavior with strong finite size effects. In view of the very limited regime of grafting density where this mean field-type extrapolation predicts thin-thick transitions at $A < 0$ the continuation of the first-order wetting transition to $A < 0$ is virtually unobservable in our simulations.

C. High grafting densities

As shown previously in Fig. 2, for $A=0$ and sufficiently high grafting densities the interface potential developed again an absolutely stable minimum indicative of autophobic dewetting of the polymer film on top of the brush consisting of identical polymers. Figure 9 shows a more detailed view of the interface potentials close to the onset of autophobicity. The depth of the minimum increases gradually as the brush becomes denser. There seems to be no evidence of related maxima in the interface potentials from visual inspection. In this case, the wetting transition that would occur as R_e^2/Σ varied while keeping $A=0$ is tricritical. At larger grafting densities the melt dewets from the brush and an attractive long-range interaction is required to stabilize a macroscopically thick liquid film.³¹ The dependence of the Hamaker constant A_{wet} on the grafting density in the autophobic regime is much stronger than in the limit of low grafting density, because the melt is displaced from the substrate and only the tails of the attractive segment-substrate interactions stabilize the melt. The inset of Fig. 9 shows a series of interface potentials obtained for a brush of $R_e^2/\Sigma=6.03$ as the Hamaker constant is increased. As a result of the long-range

TABLE II. Results for the fit of interface potentials to Eq. (18). Top: values of the coefficients a_i and b_i obtained from the fit to the linear model $C_i = a_i + b_i R_e^2/\Sigma$ (a value of $\kappa=1.2217$ is obtained for the decay rate of the exponentials). Bottom: values of the preexponential terms C_i obtained for the four interface potentials employed in the fit.

	1	2	3
a_i	-0.005 430	0.062 47	0.026 94
b_i	0.001 557	-0.016 20	0.003 134
R_e^2/Σ	C_1	C_2	C_3
5.358	0.002 914	-0.024 31	0.043 73
5.626	0.003 332	-0.028 65	0.044 57
6.028	0.003 958	-0.035 16	0.045 83
6.698	0.005 001	-0.046 01	0.047 93

forces, the stable minimum is raised, and a maximum appears leading to a first-order wetting transition at about $A_{\text{wet}}=1.1$. Since a further increase of the brush density at $A=0$ results in deeper nonwet minima and larger contact angles, we expect that the value of A required to wet a denser brush will steeply increase.

In order to locate more quantitatively the transition from critical wetting to autophobic behavior and to determine the order of the wetting transition, we again perform an analysis based on the simple model for the interface potential, Eq. (15). The difference in this case is that we do not expect the adsorbed polymers to significantly penetrate into the brush. Therefore, the adsorption of free polymers, rather than the total adsorption, is the relevant variable and we consider a model of the form

$$\beta g(\Gamma_f) = \sum_{k=1}^{\infty} C_k e^{-k\Gamma_f/\kappa}. \quad (18)$$

We find that a fit with two exponentials produces root-mean-squared deviations which are a factor of 1.4 larger than those of a fit to three exponentials, the latter providing a rather good description of the simulated data (cf. Fig. 9, full lines).

Studying the coefficients of the fit (see cf. Table II), we find that the simple model suggests that first-order wetting transitions occur for $R_e^2/\Sigma \geq 5.171$ while the wetting transition is second-order for smaller values of the grafting density. This is in agreement with the previous SCF calculations.¹⁵ The fit of the simulation data does not suggest that the location of Γ_{min} on the nonwet side of the first-order transition increases as one approaches $R_e^2/\Sigma_{\text{tcp}} \approx 5.171$ from above. We note, however, that our estimate of the transition from second- to first-order wetting has substantial uncertainties. (i) The line of first-order wetting transitions $A_{\text{wet}}(\Sigma)$ approaches $A=0$ with a very small, possibly vanishing slope. (ii) The prediction of the fit for the location of the wetting transition does not match very well the location of direct estimate obtained by the simulations at larger grafting densities. In view of the statistical accuracies of the simulation it is again very difficult to accurately locate the point which marks the end of the second-order wetting transitions and the onset of autophobicity directly from the simulation.

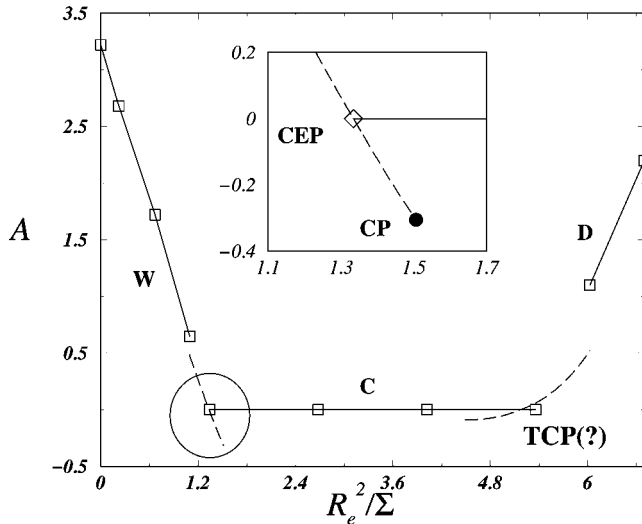


FIG. 10. Wetting phase diagram as a function of Hamaker constant A and grafting density R_e^2/Σ . The symbols are the wetting transitions as calculated from the results of this work. The full lines are a guide to the eyes. Labels W, C, and D indicate the first-order wetting transitions, second-order wetting transitions, and autophobic dewetting transitions, respectively. The dashed lines are predictions from the superposition model, Eq. (19). The inset is the phase diagram magnified in the region inside the circle.

D. Discussion of the wetting phase diagram

The full wetting phase diagram in the $A-R_e^2/\Sigma$ plane that results from the above discussion is shown in Fig. 10. The proposed methodology allows us to locate the wetting transitions directly from our simulations (empty squares). We find a direct evidence of first-order wetting transitions at low (W) and high (D) grafting densities and positive values of the effective Hamaker constant, as well as wetting of the melt on top of the brush at an intermediate range of grafting densities (C). In the latter case a second-order wetting transition occurs at $A_{\text{wet}}=0$.

It is difficult to accurately locate the grafting densities at which the wetting behavior changes and to determine the type of the wetting transition at those points. To this end we have fitted the simulation data with a simple model for the interface potential, Eqs. (15) and (18), at both ends of the line of critical wetting transitions. For finite values of A the effect of long-range interactions is accounted for by a superposition approximation. Assuming a continuous dependence of the fit parameters on the grafting density, we obtain extrapolations and we have interpreted them in a mean field style.

The superposition approximation allows us to discuss the qualitative effect of long-range interactions,

$$g(\Gamma) = g_{\text{sr}}(\Gamma) + \frac{\omega A}{\Gamma^2}, \quad (19)$$

where g_{sr} is the short-range part of the interface potential, as obtained from Eq. (15), $\omega = \frac{1}{2}(\phi_l - \phi_v)^3$ is a constant, and we have neglected the Γ^{-8} contribution. Let Γ_0 be the adsorption at the minimum of $g_{\text{sr}}(\Gamma)$. Then, taking the derivatives of $g(\Gamma)$ and expanding in a Taylor series about Γ_0 , we can obtain a first approximation for the shift of Γ_{min} due to long-range interactions,

$$\Gamma_{\text{min}}(A) = \Gamma_0 + \frac{2\omega A \Gamma_0}{g_0'' \Gamma_0^4 + 6\omega A}, \quad (20)$$

where g_0'' is the curvature of g_{sr} at Γ_0 . Given the new location of the minimum, the value of the interface potential at that point is given by

$$g(\Gamma_{\text{min}}) = g_0 + \frac{\omega A}{[\Gamma_0 + (2\omega A/g_0'' \Gamma_0^3)]^2}. \quad (21)$$

Considering that a wetting transition occurs for $g(\Gamma_{\text{min}})=0$, we find, to the first approximation,

$$A_{\text{wet}} \approx -\frac{g_0 \Gamma_0^2}{\omega [1 + (4g_0/g_0'' \Gamma_0^2)]}. \quad (22)$$

This simple result qualitatively illustrates the effect of long-range forces in the neighborhood of a first-order short-range wetting transition. Below the short-range wetting transition g_0 is negative, and long-range forces with positive A are required to wet the brush. Above the short-range wetting transition, and as long as g_{sr} exhibits a metastable minimum, long-range forces with a negative A can pull the minimum g_0 down and stabilize it.

In order to get a quantitative description of the transitions discussed above, we solve Eq. (19) numerically, using the fit to the interface potentials to interpolate or extrapolate the results as required. Included as dashed lines, Fig. 10 shows the results obtained for the wetting transitions close to the intersections of the first-order and second-order lines.

The inset of Fig. 10 magnifies the scale of the phase diagram in the region where line W meets line C. The point of intersection is a critical end point, because the second-order wetting transitions along C terminate. Below that point, at negative A , we find the continuation of line W. The transitions remain first-order, but they occur between a thin and a mesoscopic film, the latter gradually diverging as $A \rightarrow 0^-$. As we decrease A , eventually, the two states become identical and the line of transitions ends in a critical point (CP) in accord with the predictions of the SCF theory.¹⁵

From an experimental point of view, the interface potentials are usually not available and one measures either the adsorption or the contact angle. What would be the experimental signature of this complex wetting behavior? This question can be answered by employing our interface potentials along with Eqs. (4) and (7). In principle, the adsorption may be obtained as an average over a distribution of the form $P(\Gamma) \propto \exp(-\beta L_x L_y g)$. In practice, for the systems studied the expected isotherms are rounded off, because of the small lateral size and the concomitant small free energy differences. It is therefore more convenient to employ our superposition model with coefficients as obtained from the fit, Eq. (15), and determine adsorptions in the mean field sense, i.e., as the extrema of $g(\Gamma)$. From Fig. 10, we have seen that the superposition model works rather well so we expect our results to be at least semiquantitative.

Figure 11 (top) shows the adsorption isotherms for three different brushes and several values of the Hamaker constant. The left panel displays the adsorption isotherms for a brush below the critical end point (CEP) for several values of

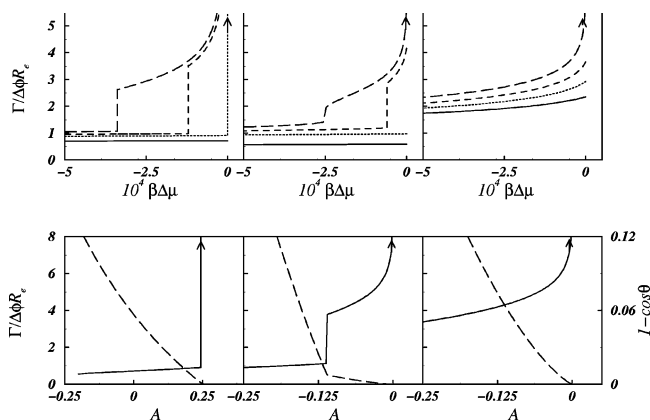


FIG. 11. Typical adsorption isotherms and contact angles in the neighborhood of the critical end point (CEP). Top: plot of adsorption vs chemical potential for three grafting densities: below the CEP ($R_c^2/\Sigma=1.206$, left), between the CEP and the CP ($R_c^2/\Sigma=1.393$, middle), and above the CP ($R_c^2/\Sigma=1.741$, right). The results are shown for several values of the Hamaker constant. From top to bottom $A=0$, and 0.1, 0.244, and 0.32 (left); $A=-0.5$, -0.2 , -8.106×10^2 , and -6.012×10^3 (middle); $A=-0.5$, -0.35 , -0.2 , and -2.0×10^3 (left). Bottom: Contact angles and adsorption at coexistence for the previously studied brushes. Contact angles in the middle figure are magnified by 10, while those of the left figure are magnified by 100.

the Hamaker constant, from $A=0$, where the brush is not wet, to A above the wetting transition. These isotherms clearly reveal the first-order nature of the transition. A similar set of results is displayed for a brush to the right of the CP. In this case, the Hamaker constant is increased from negative values towards $A=0$, and the behavior observed is typical of a second-order wetting transition. The peculiarity of the behavior described above is seen when we study brushes in between the CEP and the CP. This is displayed in the top middle panel. The isotherms obtained in this case show features common to the left and right panels. For large negative values of A , the system is not wet, and the adsorption remains small up to coexistence. However, when the continuation of the W line at negative A is crossed, a discontinuous jump is observed in the adsorption. This is very similar to a first-order wetting transition, as in the right panel. However, the adsorption does not actually diverge at coexistence, but rather remains finite, though large compared to that typical of adsorbed thin films. As $A \rightarrow 0$, the adsorption increases continuously and diverges at $A=0$, in very much the same way as the right panel. The wetting isotherm at $A=0$ may show a discontinuity, if the brush is close to the CEP, or be continuous all the way up to coexistence, for brushes beyond the CEP but yet below the CP. In the figure, we show the latter case, where the wetting isotherm at $A=0$ still displays an inflexion reminiscent of the discontinuity than can be observed for brushes of smaller grafting density.

It is important to note that the salient features described in Fig. 11 occur within an extremely small range of chemical potentials very close to coexistence. For this reason, it would be very difficult to observe them directly, either in an experiment or in our simulations. In practice, it has been found more convenient to focus either on the measurement of contact angles or on the study of adsorption at coexistence.^{23,26,28,53} In Fig. 11 (bottom), we show the calcu-

lated adsorption at coexistence as a function of Hamaker constant for the three brushes discussed previously. Again, the left and right panels show the well known behavior characteristic of first- and second-order wetting transitions. For the brush in between the CEP and the CP, however, the continuous divergence of the adsorption (second order) is preceded by a discontinuous but a finite increase (first order), a behavior known from experiments of the air/water/oil interface.²⁶ Since adsorption is related to the derivative of contact angles, the discontinuity is revealed as a change of slope in contact angle measurements. The expected values of the contact angles are displayed as dashed lines in the right ordinate axis of Fig. 11—bottom (right ordinate axis).^{54,55} Indeed, a change of slope in the contact angle is observed in the middle panel. However, the change occurs for very small contact angles of about 2° . Experimentally, the transition between the scenarios depicted in the left and middle panels, and the discontinuity in the contact angle was only measured recently.⁵³ The transition between isotherms in the middle and right panels has not yet been found, however.

The nature of the intersection between line D and line C cannot be fully elucidated by our simulations. From the extrapolation of the fit, cf. Eq. (18), a continuation of the first-order autophobic dewetting line also occurs at negative A . In that case, the intersection point would also be a critical end point. However, as noted previously, it is unlikely that the extrapolation is reliable. We rather expect that the line D ends at $A=0$ in a tricritical point.

IV. CONCLUSION

In this work we have proposed a powerful simulation technique to study wetting properties. The method determines the effective interface potential containing all thermodynamic information. From the interface potential one can determine whether the system is wet or nonwet, estimate contact angles, and infer the order of the wetting transitions. Furthermore, combining the technique with histogram reweighting one can compute adsorption isotherms and locate wetting transitions.³¹

The proposed methodology has been employed in order to study the wetting behavior of brushes varying the grafting density and strength of long-range forces. We have found that the interplay of these two control variables results in an interesting and rich wetting phase diagram, in qualitative agreement with the previous predictions of self consistent field theory.¹⁵ In the absence of long-range forces, we find transitions from nonwet to wet and back to nonwet with increasing brush density, in agreement with recent experimental observations.¹¹ The first transition is short-range first-order wetting, while the second is long-range critical wetting. Within a very small interval of brush densities beyond the short-range first-order wetting transition, the adsorption isotherm at bulk coexistence exhibits a transition from a thin to a thick layer. Increasing the grafting density further the difference between the thin and the thick state vanishes and the adsorption increases continuously as we approach the second-order wetting transition at $A=0$.

Long-range forces lead to a line of first-order wetting

transitions at low brush density, and to a line of autophobic dewetting transitions at large brush density. At negative Hamaker constants, the continuation of the former produces the line of first-order transitions between a microscopic and mesoscopic thin film discussed above. The coexistence between nonwet thin and mesoscopic films has also been found for short alkanes at the air/water interface,^{26,53} and for polystyrene on silicon wafers.²³ The very different nature of all such systems suggests that this behavior could be of a rather general nature.

ACKNOWLEDGMENTS

It is a great pleasure to thank Kurt Binder and Claudio Pastorino for stimulating discussions. One of the authors (L.G.M.) would like to thank the Universidad Complutense de Madrid and the Spanish Ministerio de Ciencia y Tecnología for the award of a Ramon y Cajal fellowship and the MCYT for financial support under Grant No. FIS2004-06227-C02-02. Another author (M.M.) received support from the priority program “Mikro- und Nanofluidik” (Mu 1674/3) and the Volkswagen foundation.

- ¹A. Cabañas, D. P. Long, and J. J. Watkins, *Chem. Mater.* **16**, 2028 (2004).
- ²M. Müller and L. G. MacDowell, *J. Phys.: Condens. Matter* **15**, R609 (2003).
- ³A. I. Milchev and A. A. Milchev, *Europhys. Lett.* **56**, 695 (2001).
- ⁴J. R. Errington, *Langmuir* **20**, 3798 (2004).
- ⁵C. Rascon and A. O. Parry, *J. Chem. Phys.* **115**, 5258 (2001).
- ⁶M. Müller, L. G. MacDowell, and A. Yethiraj, *J. Chem. Phys.* **118**, 2929 (2003).
- ⁷P. Bryk and S. Sokolowsky, *J. Chem. Phys.* **121**, 11314 (2004).
- ⁸S. Tripathi and W. G. Chapman, *J. Chem. Phys.* **112**, 094506 (2005).
- ⁹G. Reiter and R. Khanna, *Phys. Rev. Lett.* **85**, 5599 (2000).
- ¹⁰T. Kerle, R. Yerushalmi-Rosen, and J. Klein, *Europhys. Lett.* **38**, 207 (1997).
- ¹¹A. Voronov and O. Shufranska, *Langmuir* **18**, 4471 (2002).
- ¹²S. M. Sirard, R. R. Gupta, T. P. Russell, J. J. Watkins, P. F. Green, and K. P. Johnston, *Macromolecules* **36**, 3365 (2003).
- ¹³L. Leibler, A. Ajdari, A. Mourran, G. Coulon, and D. Chatenay, *OUMS Conference on Ordering in Macromolecular Systems, Osaka* (Springer-Verlag, Berlin, 1994).
- ¹⁴G. Reiter, P. Auroy, and L. Auvray, *Macromolecules* **29**, 2150 (1996).
- ¹⁵M. Müller and L. G. MacDowell, *Europhys. Lett.* **55**, 221 (2001).
- ¹⁶P. G. Ferreira, A. Ajdari, and L. Leibler, *Macromolecules* **31**, 3994 (1998).
- ¹⁷M. W. Matsen and J. M. Gardiner, *J. Chem. Phys.* **115**, 2794 (2001).
- ¹⁸J. H. Maas, G. J. Fleer, F. A. M. Leermakers, and M. Cohen-Stuart, *Langmuir* **18**, 8871 (2002).
- ¹⁹F. A. M. Leermakers, J. H. Maas, and M. Cohen-Stuart, *Phys. Rev. E* **66**, 051801 (2002).
- ²⁰A. N. Semenov, *J. Phys. II (France)* **6**, 1759 (1996).
- ²¹J. P. Wittmer, H. Meyer, J. Baschnagel, A. Johner, S. Obukhov, L. Mattioni, M. Müller, and A. N. Semenov, *Phys. Rev. Lett.* **93**, 147801 (2004).
- ²²S. P. Obukhov and A. N. Semenov, *Phys. Rev. Lett.* **95**, 038305 (2005).
- ²³P. Müller-Buschbaum, P. Vanhoorne, V. Scheumann, and M. Stamm, *Europhys. Lett.* **40**, 655 (1997).
- ²⁴M. Müller, L. G. MacDowell, P. Müller-Buschbaum, O. Wunnike, and M. Stamm, *J. Chem. Phys.* **115**, 9960 (2001).
- ²⁵P. Müller-Buschbaum, O. Wunnicke, M. Stamm, Y.-C. Lin, and M. Müller, *Macromolecules* **38**, 3406 (2005).
- ²⁶N. Shahidzadeh, D. Bonn, K. Ragil, D. Broseta, and J. Meunier, *Phys. Rev. Lett.* **80**, 3992 (1998).
- ²⁷E. Bertrand, H. Dobbs, D. Broseta, J. Indekeu, D. Bonn, and J. Meunier, *Phys. Rev. Lett.* **85**, 1282 (2000).
- ²⁸K. Ragil, J. Meunier, D. Broseta, J. O. Indekeu, and D. Bonn, *Phys. Rev. Lett.* **77**, 1532 (1996).
- ²⁹K. Binder, D. P. Landau, and M. Müller, *J. Stat. Phys.* **110**, 1411 (2003).
- ³⁰K. Binder and D. P. Landau, *Phys. Rev. B* **37**, 1745 (1988).
- ³¹L. G. MacDowell and M. Müller, *J. Phys.: Condens. Matter* **17**, S3523 (2005).
- ³²M. Müller and L. G. MacDowell, *Macromolecules* **33**, 3902 (2000).
- ³³L. G. MacDowell, P. Virnau, M. Müller, and K. Binder, *J. Chem. Phys.* **117**, 6360 (2002).
- ³⁴P. Virnau, M. Müller, L. MacDowell, and K. Binder, *J. Chem. Phys.* **121**, 2169 (2004).
- ³⁵R. Seemann, S. Herminghaus, and K. Jacobs, *J. Phys.: Condens. Matter* **13**, 4925 (2001).
- ³⁶R. Vazquez, R. Nogueira, S. Busquets, J. L. Mata, and B. Saramago, *J. Colloid Interface Sci.* **284**, 652 (2005).
- ³⁷P. Virnau, Dissertation, Johannes Gutenberg-Universität, 2003.
- ³⁸G. Torrie and J. Valleau, *J. Comput. Phys.* **23**, 187 (1977).
- ³⁹C. Borgs and R. Kotecky, *Phys. Rev. Lett.* **68**, 1734 (1992).
- ⁴⁰M. Schick *Les Houches lectures on Liquids at Interfaces* (Elsevier Science, Amsterdam, 1990), pp. 1–89.
- ⁴¹A. M. Ferrenberg and R. H. Swendsen, *Phys. Rev. Lett.* **61**, 2635 (1988).
- ⁴²M. Müller and M. Schick, *J. Chem. Phys.* **105**, 8885 (1996).
- ⁴³E. Chacon and P. Tarazona, *J. Phys.: Condens. Matter* **17**, S3493 (2005).
- ⁴⁴L. G. MacDowell, M. Müller, and K. Binder, *Colloids Surf., A* **206**, 277 (2002).
- ⁴⁵K. Binder, *Z. Phys. B: Condens. Matter* **43**, 119 (1981).
- ⁴⁶L. G. MacDowell, P. Virnau, M. Müller, and K. Binder, *J. Chem. Phys.* **120**, 5293 (2004).
- ⁴⁷Y. Djikaev, *J. Chem. Phys.* **123**, 184704 (2005).
- ⁴⁸Such minima have been predicted by self consistent field calculations (Ref. 17) and are indicative of weak first-order wetting transition. In our simulations, however, the minimum is too shallow to be resolved within the statistical accuracy and it occurs at rather large adsorption.
- ⁴⁹P. Lai and K. Binder, *J. Chem. Phys.* **97**, 586 (1992).
- ⁵⁰L. Wenning, M. Müller, and K. Binder, *Europhys. Lett.* **71**, 639 (2005).
- ⁵¹W. Zhao, G. Krausch, M. Rafailovich, and J. Sokolov, *Macromolecules* **27**, 2933 (1994).
- ⁵²S. Metzger, M. Müller, K. Binder, and J. Baschnagel, *J. Chem. Phys.* **118**, 8489 (2003).
- ⁵³E. B. S. Rafai, D. Bonn, and J. Meunier, *Phys. Rev. Lett.* **92**, 245701 (2004).
- ⁵⁴The only long-range contribution to the interface potentials stems from the explicit long-range monomer-wall interaction with strength A because all interactions are truncated. It gives rise to a term proportional to A/l^2 . Upon approaching the second-order wetting transition, $A \rightarrow 0^-$, this long-range contribution has to be balanced by an exponentially decaying short-range contribution (and not, as usual, a term which is proportional to $1/l^3$, cf. Ref. 55). Therefore, $1 - \cos \Theta$ linearly vanishes even at the second-order wetting transition in our model.
- ⁵⁵V. C. Weiss and J. O. Indekeu, *Physica A* **301**, 37 (2001).